Energy and Buildings 126 (2016) 517–523

Contents lists available at ScienceDirect

Energy and Buildings

journal homepage: www.elsevier.com/locate/enbuild

Energy and exergy analysis of different Trombe walls

Shuangping Duan[a,b], Chengjun Jing[b,*], Zhiqiang Zhao[a]

[a] Department of Civil Engineering and Architecture, Southwest University of Science and Technology, Mianyang, China
[b] Department of Architecture and Environment, Sichuan University, Chengdu, China

ARTICLE INFO

Article history:
Received 22 April 2015
Received in revised form 9 April 2016
Accepted 22 April 2016
Available online 7 May 2016

Keywords:
Trombe wall
Energy efficiency
Exergy efficiency
Solar radiation

ABSTRACT

This study aims to compare the thermal performance of two different types of Trombe wall: one with the absorber plate pasted on the thermal storage wall (Type I) and one with the absorber plate placed between the glass cover and the thermal storage wall(Type II). The glass cover is double glazed. The energy and exergy efficiencies of the Trombe walls are evaluated for various air channel depths, solar radiation intensities and the emissvities of the glass cover. The energy and exergy efficiencies, the airflow rate and air temperature rise in the air channel in the Trombe wall with the absorber plate placed between the glass cover and the thermal storage wall(Type II) are higher than those in the Trombe wall with the absorber plate pasted on the thermal storage wall(Type I). In addition, it is found that the particular exergy destruction due to absorption of the absorber plate is the largest and that a higher absorber plate temperature is preferable in decreasing the total exergy destruction and increasing exergy efficiency.

1. Introduction

One of the classical passive solar systems is the Trombe wall. A Trombe wall, which is also known as a thermal storage wall and solar heating wall [1,2], reduces a building's energy consumption by up to 30% [3] and provides thermal comfort in winter and intermediate seasons [4]. A Trombe wall is an important green architectural feature that aides the ventilation, heating and cooling of buildings.

Many theoretical and experimental studies on the performance of Trombe walls have been carried out. Khedari et al. investigated the performance of a modified Trombe wall, named the partially-glazed modified Trombe wall, which aimed to induce higher natural ventilation and provide daylight for housing [5]. The thermal performance of two types of solar facade: flat and transpired aluminum plates were compared and it was found that the transpired design was able to reduce heat losses [6]. The thermal performance of a classical Trombe wall and a composite Trombe–Michel wall was also studied [7]. It showed that the composite wall had better energy performance than the classical wall in cold and/or cloudy weather. Ryan et al. reported on test rigs resembling lightweight passive solar air-heating collectors. The thermal efficiency was shown to be a function of the heat input and the system height, but not of the channel depth [8]. The thermal performance of five different passive solar test-cells (Direct-gain, Trombe-wall, Water-wall, Sunspace, and Roofpond) was reported [9]. A research project was conducted to investigate the performance of a coupled novel triple glass and PCM wall as a solar space heater [10]. The energy performance comparison of single glass, double glass and a semi-transparent PV module integrated on the Trombe wall façade of a model test room built in Izmir, Turkey has been carried out [11]. The efficiency of the modified Trombe wall with forced convection that could be operated in four different modes was analyzed [12]. A PV-Trombe wall, installed in a fenestrated room with heat storage, was investigated to approach the practical application of this type of solar wall [13].

Most of the studies on Trombe walls were based on the energy balance equations. However, the energy balance equations alone do not consider the internal losses, and the energy efficiency is not an adequate criterion for Trombe walls. Exergy analysis can reflect the quality change of solar energy transfer process, use and consumption through Trombe walls. Exergy analysis is more informative with regard to the optimum operating zone, quantifying the inefficiencies, their relative magnitudes and locations [14–16]. Exergy is the maximum work potential that can be obtained from a form of energy [17]. Exergy efficiency is more realistic than energy efficiency, and exergy analysis should be considered in the evaluation and comparison of solar thermal systems [18]. Therefore, the main consideration in this study will be on the detailed energy and exergy analysis of two types of Trombe walls, one of which has the absorber plate pasted on the thermal storage wall (Type I) and the other of which has the absorber plate placed between

* Corresponding author at: Sichuan University, No.24 South Section 1, Yihuan Road, Chengdu, China.
E-mail address: chengjunjing@126.com (C. Jing).

http://dx.doi.org/10.1016/j.enbuild.2016.04.052
0378-7788/

the glass cover and the thermal storage wall (Type II). These are for evaluating the performance and optimizing the designed Trombe walls with the maximum exergy efficiency under given operating conditions.

2. The description of Trombe walls

In Fig. 1, the physical model for the two types of Trombe walls is divided as follows: the glass cover, the absorber plate, the air channel, the thermal storage wall and two openings. Two openings are respectively located on the upper and lower part of the thermal storage wall. In Fig. 1(a), the absorber plate is pasted on the thermal storage wall (Type I) and there exists an air channel between the glass cover and the absorber plate. In Fig. 1(b), the absorber plate is placed between the glass cover and the thermal storage wall (Type II) with the air channel between the absorber plate and the thermal storage wall, so there is an air gap between the glass cover and the absorber plate. The glass cover is double glazed in Fig. 1. Solar radiation penetrates through the glass cover and is absorbed by the absorber plate which results in a temperature rise of the absorber plate. Colder air from indoor enters the air channel through the lower opening, and is heated by the hot absorber plate and rises and then enters indoors through the upper opening. The heat transfer modes and heat exchange in the system are shown in Fig. 1.

3. Energy analysis

While the energy balance equations are derived, some assumptions have been made:

(1) The systems operate under steady state conditions.
(2) The air temperature in air channel changes only in the direction of the flow.
(3) Heat transfer through the glass cover, the absorber plate, and the thermal storage wall is 1-D and in the direction perpendicular to the air flow.
(4) The heat loss of the lateral walls is neglected due to its small effect.

For the studied Trombe walls shown in Fig. 1, the energy balance equations are written as below.

The glass cover is double glazed which has four surfaces and one air layer. The energy balance equations for the first and second surfaces of the glass cover are:

$$h_{cga}A_g(T_{g1}-T_a)+h_{rgs}A_g(T_{g1}-T_a)+\frac{\lambda_g}{\delta_g}A_g(T_{g1}-T_{g2}) = \alpha_g A_g I \quad (1)$$

$$(h_{rgg}+\frac{\lambda_{fg}}{\delta_{fg}})A_g(T_{g2}-T_{g3})+\frac{\lambda_g}{\delta_g}A_g(T_{g2}-T_{g1})=0 \quad (2)$$

where T_{g1}, T_{g2}, T_{g3} are respectively the temperatures of the first, second and third surfaces of the double glazing shown in Fig. 1 (°C), T_a is the outdoor temperature (°C), A_g is the area of the double glazing (m^2), I is the solar radiation intensity(W/m^2), α_g is the absorptivity of the glass cover, λ_g, λ_{fg} are respectively the thermal conductivity of the glass and air in the air layer(W/m·K), δ_g, δ_{fg} are respectively the thicknesses of the glass and the air layer(m).

The convection heat transfer coefficient due to wind h_{cga} is given by W.H. Mcadams as [19]:

$$h_{cga}=5.7+3.8u_w$$

where u_w is the wind speed.

The radiation heat transfer coefficient h_{rgs} from the outside surface of the double glazing to the sky referred to the ambient temperature is obtained from

$$h_{rgs}=\frac{\sigma_b\varepsilon_{g1}({T_{g1}}^4-{T_s}^4)}{T_{g1}-T_a}$$

where σ_b is Stefan–Boltzmann constant ($5.67\times10^{-8}W/m^2\cdot K^4$), and ε_{g1} is the emissivity of the first surface of the glass cover.

The sky temperature T_s is given by Duffie and Beckman [20] as

$$T_s=0.0552T_a^{1.5}$$

The radiation heat transfer coefficient h_{rgg} from the third surface to the second surface of the double glazing can be derived as

$$h_{rgg}=\frac{\sigma({T_{g3}}^2+{T_{g2}}^2)(T_{g3}+T_{g2})}{\frac{1}{\varepsilon_{g3}}+\frac{1}{\varepsilon_{g2}}-1}$$

where ε_{g2}, ε_{g3} are respectively the emissivities of the second and third surfaces of the double glazing.

The energy balance equations for the third and fourth surfaces of the double glazing are:

$$(h_{rgg}+\frac{\lambda_{fg}}{\delta_{fg}})A_g(T_{g3}-T_{g2})+\frac{\lambda_g}{\delta_g}A_g(T_{g3}-T_{g4})=\alpha_g A_g\tau_g I \quad (3)$$

$$(h_{rpg}+\frac{\lambda_{fp}}{\delta_{fp}})A_p(T_{g4}-T_p)+\frac{\lambda_g}{\delta_g}A_g(T_{g4}-T_{g3}) +h_{cg}A_g(T_{g4}-T_f)=0 \quad (4)$$

where T_{g4} is the temperature of the fourth surface of the double glazing, T_p,T_f are respectively the temperatures of the absorber plate and air in air channel (°C), A_p is the area of the absorber plate (m^2),τ_g is the transmissivity of the double glazing, λ_{fp} is the thermal conductivity of air in air layer between the absorer plate and the glass cover (W/m·K), δ_{fp} is the thickness of the air layer (m).

The radiation heat transfer coefficient h_{rpg} from the absorber plate to the fourth surface of the double glazing can be obtained from

$$h_{rpg}=\frac{\sigma({T_p}^2+{T_{g4}}^2)(T_p+T_{g4})}{\frac{1}{\varepsilon_p}+\frac{1}{\varepsilon_{g4}}-1}$$

where ε_p, ε_{g4} are respectively the emissivities of the fourth surface of the double glazing and the absorber plate.

The convection heat transfer coefficient h_{cg} between the air in the air channel and the fourth surface of the double glazing can be defined as

$$h_{cg}=Nu\lambda_f/\delta$$

where λ_f is the heat conduction coefficient of air in air channel (W/m·K), δ is the thickness of the air channel (m). Nu is Nusselt number.

In Eq. (4), $\lambda_{fp}/\delta_{fp}=0$ for the first type of Trombe wall shown in Fig. 1(a); $h_{cg}=0$ for the second type of Trombe wall shown in Fig. 1(b). The heat balance equation for the absorber plate is:

$$h_{cp}A_p(T_p-T_f)+(h_{rpg}+\frac{\lambda_{fp}}{\delta_{fp}})A_p(T_p-T_{g4})+U_pA_p(T_p-T_n) +h_{rpw}A_p(T_p-T_w)=\alpha_p\tau_g A_p I \quad (5)$$

where T_w is the temperature of the thermal storage wall (°C), T_n is the indoor temperature (°C).

The radiation heat transfer coefficient h_{rpw} from the absorber plate to the thermal storage wall can be obtained from

$$h_{rpw}=\frac{\sigma({T_p}^2+{T_w}^2)(T_p+T_w)}{\frac{1}{\varepsilon_p}+\frac{1}{\varepsilon_w}-1}$$

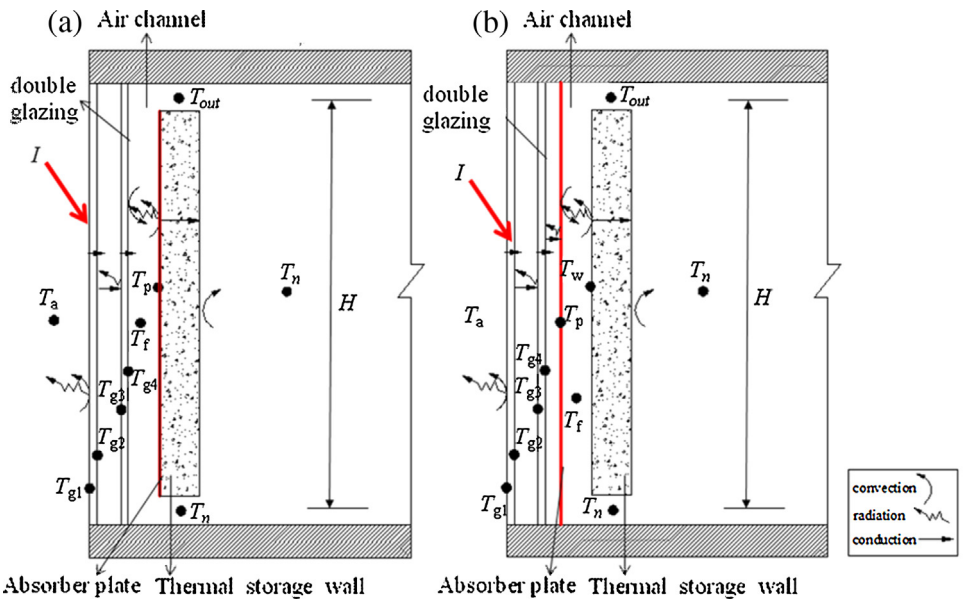

Fig. 1. Physical model of Trombe wall. (a)Type I: the absorber plate pasted on the thermal storage wall; (b) Type II: the absorber plate placed between the glass cover and the thermal storage wall.

where ε_w is the emissivity of the outside surface of the thermal storage wall.

The heat transfer coefficient U_p through the thermal storage wall is given as

$$U_p = \frac{1}{\frac{\delta_w}{\lambda_w} + \frac{\delta_{in}}{\lambda_{in}} + \frac{1}{h_n}}$$

where λ_w, λ_{in} are respectively the heat conduction coefficients of the thermal storage material and thermal insulation material (W/m·K), δ_w , δ_{in} are respectively the thicknesses of the thermal storage and insulation layers (m), h_n is the convection heat transfer coefficient between the thermal storage wall and indoor air (W/m^2·K).

The convection heat transfer coefficient h_{cp} between the air in air channel and the absorber plate may be defined as

$$h_{cp} = Nu\lambda_f/\delta$$

In Eq. (5), $\lambda_{fp}/\delta_{fp} = 0$, $h_{rpw} = 0$ for the first type of Trombe wall shown in Fig. 1(a); $U_p = 0$ for the second type of Trombe wall shown in Fig. 1(b).

The energy balance equation for the air in the air channel is:

$$h_{cp}A_p(T_p - T_f) + h_{cg}A_g(T_{g4} - T_f) + h_{cw}A_w(T_w - T_f) = \rho_f q c_p(T_{out} - T_n) \quad (6)$$

where ρ_f is the air density(kg/m^3), q is the airflow rate (m^3/s), c_p is the specific heat of air(J/kg·K), T_{out} is the outlet air temperature (°C).

The convection heat transfer coefficient h_{cw} between the air in air channel and the thermal storage wall in Fig. 1(b) can be defined as

$$h_{cw} = Nu\lambda_f/\delta$$

In Eq. (6), $h_{cw} = 0$ for the first type of Trombe wall shown in Fig. 1(a); $h_{cg} = 0$ for the second type of Trombe wall shown in Fig. 1(b).

The mean air temperature in air channel is calculated [21].

$$T_f = \gamma T_{out} + (1-\gamma)T_n$$

where $\gamma = 0.74$

In Fig. 1(b), the heat balance equation for the outside surface of thermal storage wall is:

$$h_{cw}A_w(T_w - T_f) + U_pA_b(T_w - T_n) + h_{rpw}A_p(T_w - T_p) = 0 \quad (7)$$

where A_w is the area of the thermal storage wall (m^2).

The airflow rate q can be derived as

$$q = c_d A^* \sqrt{2gH\frac{|T_{out} - T_n|}{T_n}} \quad (8)$$

where c_d is the discharge coefficient, $c_d = 0.57$ [22], A^* is the effective area of the openings (m^2), $A^* = \sqrt{2}A_tA_b/\sqrt{A_b^2 + A_t^2}$, A_t and A_b are respectively the areas of the upper opening and the lower opening (m^2), H is the vertical distance of two openings (m).

The Nusselt number for laminar ($6000 < Ra \le 2 \times 10^5$) and turbulent ($2 \times 10^5 < Ra < 1.1 \times 10^7$) natural convection flow is calculated by using the Eqs. (9) and (10), respectively [23].

$$Nu = 0.197Ra^{\frac{1}{4}}(\delta/H)^{\frac{1}{9}} \quad (9)$$

$$Nu = 0.073Ra^{\frac{1}{3}}(\delta/H)^{\frac{1}{9}} \quad (10)$$

where $Ra = GrPr$, $Gr = g\beta\delta^3\Delta T/\nu_f^2$, $Pr = \lambda_f/\rho_f c_p \nu_f$, β is the coefficient of thermal expansion (K^{-1}), ΔT is the temperature difference of surfaces (°C).

The density, thermal conductivity, and kinematic viscosity coefficient of air can be obtained from the equations below [24].

$$\rho_f = 1.1614 - 0.00353(T_f - 300)$$

$$\lambda_f = 0.0263 + 0.000074(T_f - 300)$$

$$\nu_f = [1.846 + 0.00472(T_f - 300)] \times 10^{-5}/\rho_f$$

$$c_p = 1007 + 0.04(T_f - 300)$$

The total heat supply from Trombe walls is given below.

For Fig. 1(a):

$$Q_z = \rho_f q c_p(T_{out} - T_n) + U_pA_p(T_p - T_n) \quad (11)$$

For Fig. 1(b):

$$Q_z = \rho_f q c_p (T_{out} - T_n) + U_p A_w (T_w - T_n) \tag{12}$$

The energy efficiency of Trombe wall is defined as

$$\eta_1 = \frac{Q_z}{IA_p} \tag{13}$$

4. Exergy analysis

The exergy balance equation for a Trombe wall can be written as:

$$Ex_{sun} + Ex_{in} - Ex_{out} = Ex_{dest} \tag{14}$$

where Ex_{sun} is the solar exergy(W), Ex_{in} is the inlet exergy(W), Ex_{out} is the outlet exergy (W), Ex_{dest} is the exergy destruction(W).

Solar exergy Ex_{sun} can be introduced as [25]:

$$Ex_{sun} = IA_g(1 - \frac{T_a}{T_{sun}}) \tag{15}$$

Considering that the effective sun temperature T_{sun} is 3/4 sun temperature as black body, T_{sun} = 4500 K [26].

Useful exergy Ex_u is the amount of increase in exergy level of the air leaving the lower opening.

$$Ex_u = Ex_{out} - Ex_{in} = \rho_f q[c_p(T_{out} - T_n) - T_a(c_v Ln\frac{T_{out}}{T_n} - R\ln\frac{\rho_{out}}{\rho_n})] \tag{16}$$

where ρ_n is the inlet air density (kg/m^3), ρ_{out} is the outlet air density (kg/m^3), c_v is the constant-volume specific heat of air (J/kg·K), R is the gas constant (J/kg·K).

Eq. (16) gives the kinetic energy (exergy) transferred by free convection to the air channel. The amount of exergy gets transferred into the kinetic energy of the air flow, thereby offsetting high-quality electricity (pure exergy) that would power fans.

On the other hand, the total exergy destruction may be divided into the following parts.

For the first type of Trombe wall shown in Fig. 1(a),

$$Ex_{dest} = Ex_{dest,1} + Ex_{dest,2} + Ex_{dest,3} + Ex_{dest,4} + Ex_{dest,5a} + Ex_{dest,6a} + Ex_{dest,7a}$$

For the second type of Trombe wall shown in Fig. 1(b),

$$Ex_{dest} = Ex_{dest,1} + Ex_{dest,2} + Ex_{dest,3} + Ex_{dest,4} + Ex_{dest,5b} + Ex_{dest,6b} + Ex_{dest,7b} + Ex_{dest,8}$$

Ignoring the exergy destruction due to fluid friction, exergy destruction from the double glazing are due to glass emission and heat convection, so

$$Ex_{dest,1} = \varepsilon_{g1}\sigma_b A_g(T_{g1}^4 - T_a^4)(1 - \frac{T_a}{T_{g1}}) + h_{cga}A_g(T_{g1} - T_a)(1 - \frac{T_a}{T_{g1}}) \tag{17}$$

On the right hand side of Eq. (17), the first term is the exergy destruction due to glass emission, and the second term is the exergy destruction due to heat convection.

Exergy destruction due to absorption of the glass cover:

$$Ex_{dest,2} = IA_g\alpha_g(\frac{T_a}{T_{g1}} - \frac{T_a}{T_{sun}}) + IA_g\tau_g\alpha_g(\frac{T_a}{T_{g3}} - \frac{T_a}{T_{sun}}) \tag{18}$$

In the right hand in Eq. (18), the first term is exergy destruction due to absorption of the first layer glass, the second term is exergy destruction due to absorption of the second layer glass.

Exergy destruction due to radiation and heat conduction of the double glazing is:

$$Ex_{dest,3} = \frac{\lambda_g}{\delta_g}A_g(T_{g2} - T_{g1})(\frac{T_a}{T_{g1}} - \frac{T_a}{T_{g2}}) + \frac{\lambda_g}{\delta_g}A_g(T_{g4} - T_{g3})(\frac{T_a}{T_{g3}} - \frac{T_a}{T_{g4}}) + \frac{\lambda_{fg}}{\delta_{fg}}A_g(T_{g3} - T_{g2})(\frac{T_a}{T_{g2}} - \frac{T_a}{T_{g3}}) + \frac{\sigma_b A_g(T_{g3}^4 - T_{g2}^4)}{1/\varepsilon_{g2} + 1/\varepsilon_{g3} - 1}(\frac{T_a}{T_{g2}} - \frac{T_a}{T_{g3}}) \tag{19}$$

In the right hand side of Eq. (19), the first,second and third terms are respectively exergy destruction due to heat conduction of the first layer, second layer glass and air gap, the fourth term is the exergy destruction due to radiation between the second and third surfaces of the double glazing.

Exergy destruction due to absorption of the absorber plate is:

$$Ex_{dest,4} = IA_p\tau_g\alpha_s(\frac{T_a}{T_p} - \frac{T_a}{T_{sun}}) \tag{20}$$

In Fig. 1(a), exergy destruction due to convection between the air in channel and the fourth surface of the double glazing, the absorber plate:

$$Ex_{dest,5a} = T_a[\rho_f q c_p Ln\frac{T_{out}}{T_n} - \frac{Q_1}{T_{g4}} - \frac{Q_2}{T_p}] \tag{21}$$

where $Q_1 + Q_2 = \rho_f q c_p(T_{out} - T_n)$, $Q_1 = h_{cg}A_g(T_{g4} - T_f)$,$Q_2 = h_{cp}A_p(T_p - T_f)$

In Fig. 1(b), exergy destruction due to convection between the air in channel and the absorber plate, the external surface of the thermal storage wall is:

$$Ex_{dest,5b} = T_a[\rho_f q c_p Ln\frac{T_{out}}{T_n} - \frac{Q_1}{T_w} - \frac{Q_2}{T_p}] \tag{22}$$

where $Q_1 = h_{cw}A_w(T_w - T_f)$, $Q_2 = h_{cp}A_p(T_p - T_f)$

In Fig. 1(a), exergy destruction due to radiation between the absorber plate and the fourth surface of the double glazing is:

$$Ex_{dest,6a} = \frac{\sigma_b A_p({T_p}^4 - {T_{g4}}^4)}{\frac{1}{\varepsilon_p} + \frac{1}{\varepsilon_{g4}} - 1}(\frac{T_a}{T_{g4}} - \frac{T_a}{T_p}) \tag{23}$$

In Fig. 1(b), exergy destruction due to radiation and conduction between the absorber plate and the fourth surface of the double glazing is:

$$Ex_{dest,6b} = [\varepsilon_p\sigma_b A_p({T_p}^4 - {T_{g4}}^4) + \frac{\lambda_{fp}}{\delta_{fp}}A_p(T_p - T_{g4})](\frac{T_a}{T_{g4}} - \frac{T_a}{T_p}) \tag{24}$$

In Fig. 1(a), exergy destruction due to heat transfer between the absorber plate and indoor air is:

$$Ex_{dest,7a} = U_p A_p(T_p - T_n)(\frac{T_a}{T_n} - \frac{T_a}{T_p}) \tag{25}$$

In Fig. 1(b), exergy destruction due to heat transfer between the external surface of the thermal storage wall and indoor air is:

$$Ex_{dest,7b} = U_p A_p(T_w - T_n)(\frac{T_a}{T_n} - \frac{T_a}{T_w}) \tag{26}$$

In Fig. 1(b), exergy destruction due to radiation between the absorber plate and the outside surface of the thermal storage wall is:

$$Ex_{dest,8} = \varepsilon_p\sigma_b A_p(T_p^4 - T_w^4)(\frac{T_a}{T_w} - \frac{T_a}{T_p}) \tag{27}$$

Finally, the exergy efficiency is given as

$$\eta_2 = \frac{Ex_u}{Ex_{sun}} = \frac{\rho_f q c_p(T_{out} - T_n - T_a Ln\frac{T_{out}}{T_n})}{IA_g(1 - \frac{T_a}{T_{sun}})} \tag{28}$$

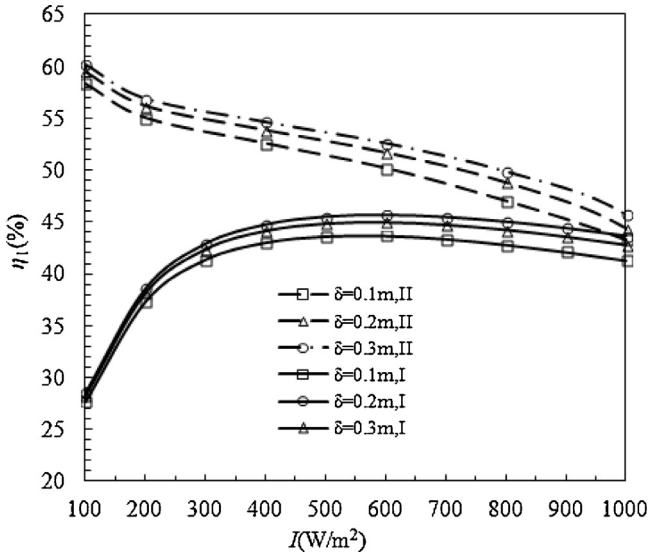

Fig. 2. Variation of energy efficiency with channel depth and solar intensity for two types of Trombe walls.

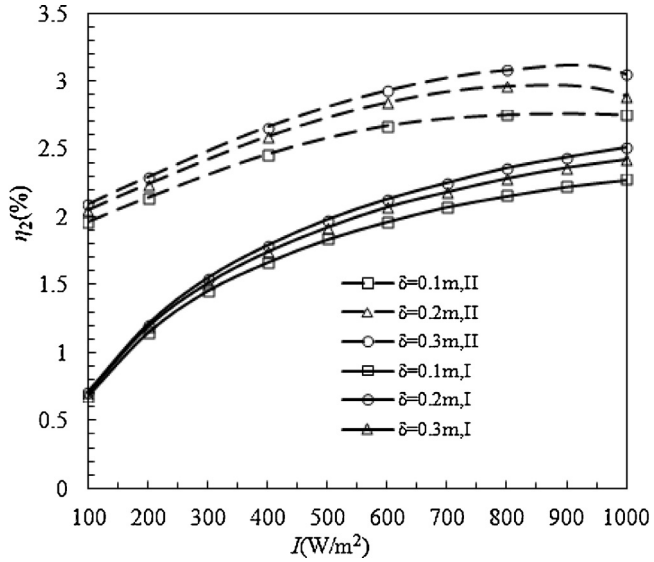

Fig. 3. Variation of exergy efficiency with channel depth and solar intensity for two types of Trombe walls.

5. Results and discussion

As a numerical example, it is assumed that T_a = 278 K, T_n = 287 K. The glass cover is 3 m height and 3 m wide, which has two layer glass 0.006m(λ_g = 0.65W/m·K) and one layer air 0.012 m in thickness. The dimensions of the upper and lower openings are 0.2 m × 2.0 m. The thickness of the air channel is 0.1 m, 0.2 m and 0.3 m. The transmissivity and absorptivity of glass are respectively 0.85 and 0.05. The absorptivity and emissivity of the absorber plate are respectively 0.95 and 0.85. The thermal storage wall is made up of reinforced concrete (λ_w = 1.547W/m·K) and insulating material(λ_{in} = 0.047W/m·K).

The temperatures(T_{g1},T_{g2},T_{g3},T_{g4},T_p,T_f,T_w) and airflow rate in Eqs. (1)–(8) are solved by an iteration method, and the iteration process continues until the convergence value 10^{-6}. The energy efficiency, solar exergy, useful exergy, exergy destruction and exergy efficiency are solved by substituting the obtained temperatures into Eqs. (13)–(28). The results are shown in Figs. 2–6 . Numerical results are presented for the effect of different parameters on the thermal performance of Trombe walls with natural convection flow. The parameters include air channel depth, solar radiation intensity, emissivity of the glass cover.

5.1. The effect of solar radiation intensity

Figs. 2 and 3 show the variation of energy efficiency and exergy efficiency with solar radiation intensity for the two types of Trombe walls. From Fig. 2 and Fig. 3, for the first type of Trombe wall (Type I), with the increase of solar radiation intensity up to a certain point, the energy and exergy efficiencies increase and reach maximum values. With further increase in solar radiation intensity, the energy efficiency decreases. The highest energy efficiency is found at solar radiation intensity of around 600 W/m^2. However, the exergy efficiency reaches its maximum value when the solar radiation intensity is more than 1000W/m^2, which can be deduced from Fig. 3.

For the second type of Trombe wall(Type II), the energy efficiency decreases with solar radiation intensity and a negative relationship between energy efficiency and solar radiation intensity was observed, as shown in Fig. 2. From Fig. 3, with the increase of solar radiation intensity, the exergy efficiency first rises slowly and then decreases. It is found that the highest exergy efficiency exists at a solar radiation intensity of around 900 W/m^2.

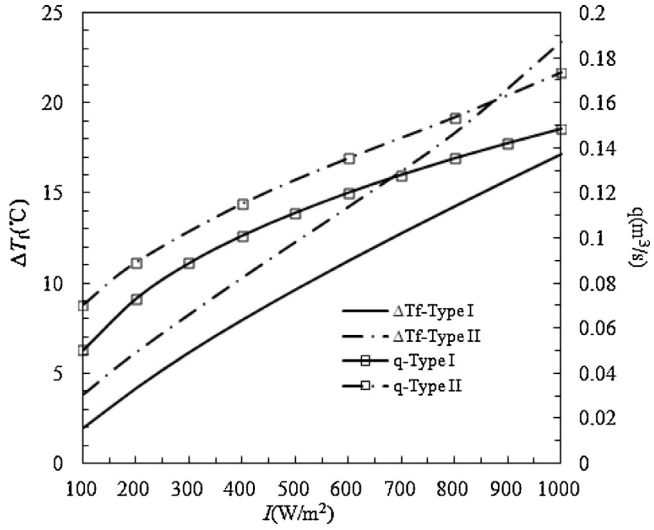

Fig. 4. Variation of airflow rate and air temperature rise increase with solar intensity for two types of Trombe walls when δ = 0.1m.

5.2. The effect of air channel depth

From Fig. 2 and Fig. 3, both the energy efficiency and exergy efficiency increase slowly with air channel depth for the two types of Trombe walls for the given solar radiation intensity. With the increase of air channel depth, the cross-sectional flow area of the air channel increases, and buoyancy forces overcome the friction forces and cause the mass flow rate to rise in the air channel. Hence, the air velocity and consequently heat transfer coefficient are increased. The heat transfer rate to the air flow and consequently the energy efficiency and the outlet temperature of air flow will increase because of the better convection heat transfer between air in the air channel and solid walls. The exergy efficiency is dependent on the reciprocal effects of the energy efficiency and outlet air temperature. Hence, the exergy efficiency increases with the channel depth.

Table 1
Energy and exergy analysis of Trombe walls ($\delta = 0.1m$).

Trombe Wall	I (kW/m^2)	Ex_{solar} (kW)	Ex_u (kW)	$Ex_{dest,1}$ (kW)	$Ex_{dest,2}$ (kW)	$Ex_{dest,3}$ (kW)	$Ex_{dest,4}$ (kW)	$Ex_{dest,5}$ (kW)	$Ex_{dest,6}$ (kW)	$Ex_{dest,7}$ (kW)	η_1(%)	η_2(%)
Type I	0.1	0.844	0.006	0.000	0.142	0.007	0.597	0.006	0.004	0.001	27.69	0.67
	0.2	1.689	0.019	0.007	0.278	0.012	1.127	0.034	0.016	0.002	37.36	1.14
	0.4	3.378	0.056	0.056	0.530	0.019	2.045	0.148	0.057	0.004	43.01	1.66
	0.6	5.066	0.099	0.148	0.760	0.025	2.831	0.308	0.110	0.005	43.65	1.96
	0.8	6.755	0.145	0.290	0.970	0.031	3.518	0.492	0.169	0.006	42.79	2.15
	1	8.444	0.192	0.487	1.161	0.038	4.129	0.683	0.233	0.007	41.27	2.27
Type II	0.1	0.844	0.017	0.004	0.076	0.012	0.669	0.029	0.007	0.002	58.28	1.96
	0.2	1.689	0.036	0.024	0.146	0.017	1.255	0.089	0.020	0.003	55.01	2.14
	0.4	3.378	0.083	0.090	0.275	0.026	2.246	0.275	0.063	0.005	52.55	2.46
	0.6	5.066	0.135	0.210	0.386	0.036	3.040	0.515	0.134	0.006	50.18	2.67
	0.8	6.755	0.186	0.422	0.480	0.046	3.654	0.768	0.242	0.007	47.02	2.75
	1	8.444	0.232	0.794	0.556	0.056	4.100	0.984	0.394	0.009	43.26	2.75

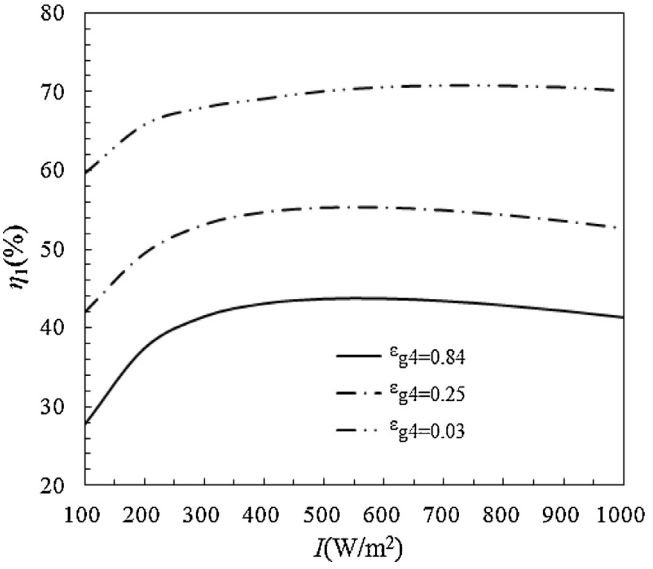

Fig. 5. Variation of energy efficiency with emissivity for the first type of Trombe wall when $\delta = 0.1$m.

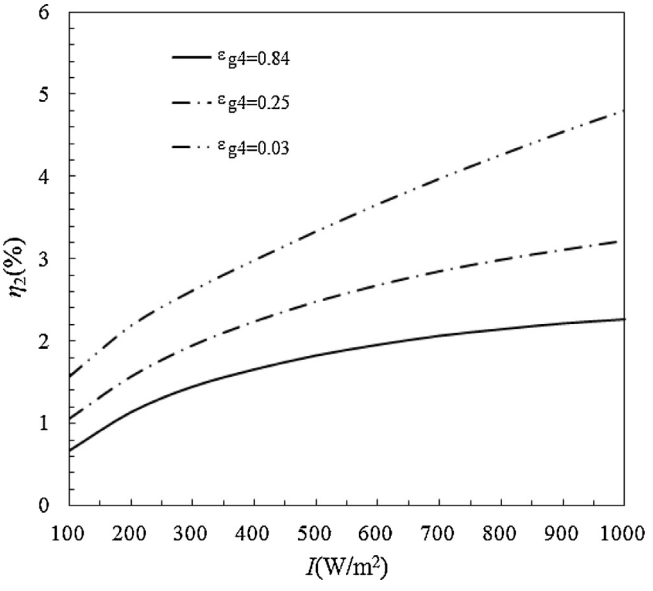

Fig. 6. Variation of exergy efficiency with emissivity for the first type of Trombe wall when $\delta = 0.1$m.

5.3. Comparison between two types of Trombe walls

From Fig. 2 and Fig. 3, it is also found that the energy and exergy efficiencies of the second type of Trombe wall (Type II) are higher than those of the first type of Trombe wall (Type I) at the same solar radiation intensity and air channel depth, which are also shown in Table 1. In addition, Fig. 4 shows variation of the airflow rate and the air temperature rise in the air channel with solar radiation intensity for the two types of Trombe walls when $\delta = 0.1m$ and the emissivities of the four surfaces of the double glazing are 0.84. From Fig. 4, the airflow rate and air temperature rise increase with solar radiation intensity. At the same solar radiation intensity, both the airflow rate and air temperature rise in the second type of Trombe wall (Type II) exceed those in the first type of Trombe wall (Type I).

5.4. The effect of emissivity of the glass cover

Fig. 5 and 6 present both the energy and exergy efficiencies at various solar intensities and emissivities when $\delta = 0.1$m for the first type of Trombe wall (Type I). As examples, the emissivities of the fourth surfaces of the double glazing are set to different values. With a decrease in emissivity which reduces the radiation heat losses of Trombe wall, the energy and exergy efficiencies increase greatly. Moreover, the emissivity of the fourth surface of the double glazing has a more important effect on the energy and exergy efficiencies than that of other three surfaces of the double glazing. That is due to the fact that the radiation heat transfer between the glass cover and the absorber is predominant. Therefore, a decrease in emissivity of the fourth surface which results in the reduction of this part of radiation heat loss is an effective method to increase the energy and exergy efficiencies.

5.5. Exergy destruction

Although the energy efficiency is relatively high for two types of Trombe walls, the exergy efficiency is very low. This is because the exergy destruction is too high in the exergy transfer. From Table 1, the exergy destruction due to absorption of the absorber plate is the largest among all types of exergy destruction. The exergy destruction due to absorption of the glass cover, the exergy destruction due to convection between air in the air channel and the solid walls(the glass cover and the absorber plate) also account for the great proportion. Other forms of exergy destruction are lower. Hence, a reduction in exergy destruction due to absorption of the absorber plate can cause a remarkable increase in the exergy efficiency. It can also be seen from Eq. (22), in order to decrease the exergy destruction due to absorption of the absorber plate and increase the exergy efficiency, the better way is to increase the temperature of the absorber plate.

6. Conclusions

The thermal performances of two types of Trombe walls with natural convection flow have been studied through mathematical model. From the viewpoints of the first and second laws of thermodynamics, the effect of various parameters such as air channel depth, solar radiation intensity and emissivity of the glass cover on the energy efficiency, exergy efficiency, exergy destruction, the airflow rate and the air temperature rise was analyzed. It is concluded that the second type of Trombe wall has better thermal performance compared to the first type of Trombe wall. In the second type of Trombe wall (Type II), the energy and exergy efficiencies are greater than those in the first type of Trombe wall (Type I) under the same operational conditions. This is because the second type of Trombe wall is able to reduce the convection and radiation heat losses and thus there are more convection heat flow to air in the air channel and higher air temperature rise and airflow rate. Solar radiation intensity and the emissivity of the glass cover have a great effect on the thermal performance of the systems. The energy efficiencies of the two types of Trombe walls are relatively high, but exergy efficiency is very low. The exergy destruction due to absorption of the absorber plate is the largest. The increase in the temperature of the absorber plate is an effective method to decrease exergy destruction and increase energy and exergy efficiencies.

Acknowledgements

The authors gratefully acknowledge the funding by the Natural Scientific Foundation of China(51208442).

References

[1] K. Hami, B. Draoui, O. Hami, The thermal performances of a solar wall, Energy 39 (2012) 11–16.
[2] X. Fang, T. Yang, Regression methodology for sensitivity analysis of solar heating walls, Appl. Therm. Eng. 28 (2008) 2289–2294.
[3] M.F. Hordeski, New Technologies for Energy Efficiency, The Fairmont Press, New York, 2011.
[4] Francesca Stazi, Alessio Mastrucci, Costanzo di Perna, The behavior of solar walls in residential buildings with different insulation levels: an experimental and numerical study, Energy Build. 47 (2012) 217–229.
[5] J. Khedari, C. Pongsatirat, W. Puangsombut, J. Hirunlabh, Experimental performance of partially-glazed modified Trombe wall, Int. J. Ambient Energy 26 (2005) 27–36.
[6] Hoy Yen Chan, Jie Zhu, Mohd Hafidz Ruslan, Kamaruzzaman Sopian, Saffa Riffat, Thermal analysis of flat and transpired solar facades, Energy Procedia 48 (2014) 1345–1354.
[7] Jibao Shen, Ste phane Lassue, Laurent Zalewski, Dezhong Huang, Numerical study on thermal behavior of classical or composite Trombe solar walls, Energy Build. 39 (2007) 962–974.
[8] D. Ryan, S.A.M. Burek, Experimental study of the influence of collector height on the steady state performance of a passive solar air heater, Sol. Energy 84 (2010) 1676–1684.
[9] Alfredo Fernaíndez-Gonzaílez, Analysis of the thermal performance and comfort conditions produced by five different passive solar heating strategies in the United States Midwest, Sol. Energy 81 (2007) 581–593.
[10] Yusuf Ali Kara, Aslıhan Kurnuc, Performance of coupled novel triple glass and phase change material wall in the heating season: an experimental study, Sol. Energy 86 (2012) 2432–2442.
[11] Basak Kundakci Koyunbaba, Zerrin Yilmaz, The comparison of Trombe wall systems with single glass, double glass and PV panels, Renew. Energy 45 (2012) 111–118.
[12] S. Dragicevic, M. Labic, Influence of constructive and operating parameters on a modified Trombe wall efficiency, Arch. Civ. Mech. Eng. 11 (2011) 825–838.
[13] J. Jie, Y. Hua, P. Gang, L. Jianping, Study of PV-Trombe wall installed in a fenestrated room with heat storage, Appl. Therm. Eng. 27 (2007) 1507–1515.
[14] L.T. Kostic, T.M. Pavlovic, Z.T. Pavlovic, Influence of reflectance from flat aluminum concentrators on energy efficiency of PV/thermal collector, Appl. Energy 87 (2010) 410–416.
[15] S. Farahat, F. Sarhaddi, H. Ajam, Exergetic optimization of flat plate solar collectors, Renew. Energy 34 (2009) 1169–1174.
[16] E. Torres-Reyes, J.J. Navarrete-Gonzalez, J.G. Cervantes-de Gortari, Thermodynamic optimization as an effective tool to design solar heating systems, Energy 29 (2004) 2305–2315.
[17] A. Bejan, Advanced Engineering Thermodynamics, Wiley InterScience Pub, 2006.
[18] H.H. Ozturk, Y. Demirel, Exergy-based performance analysis of packed-bed solar air heaters, Int. J. Energy Res. 28 (2004) 423–432.
[19] W.H. Mcadams, Heat Transmission, 3rd ed., McGraw-Hill, New York, 1994.
[20] J.A. Duffie, W.A. Beckman, Solar Thermal Process, John Wiley & Sons Inc., New York, 1974.
[21] J. Hirunlabh, W. Kongduang, P. Namprakai, et al., Study of natural ventilation of houses by a metallic solar wall under tropical climate, Renew. Energy 18 (1999) 9–19.
[22] A. Akbarzadeh, W.W.S. Charters, D.A. Lesslie, Thermo circulation characteristics of a Trombe wall passive test cell, Sol. Energy 28 (1982) 461–468.
[23] Z.X. Min, X.P. Ren, F.M. Mei, Heat Transmission, 3rd ed., Architecture Publishing Company of China, Beijing, 2000.
[24] F.P. Incropera, D.P. Dewitt, Fundamentals of Heat and Mass, 4th ed., John Wiley & Sons Inc., New York, 1996.
[25] K.K. Dutta Gupta, S. Saha, Energy analysis of solar thermal collectors, Renew. Energy Environ. 103 (1990) 283–287.
[26] A. Bejan, D.W. Keary, F. Kreith, Second law analysis and synthesis of solar collector systems, J. Sol. Energy Eng. 103 (1981) 23–28.